Solution Structure of a Human Cystatin A Variant, Cystatin A^{2-98} M65L, by NMR Spectroscopy. A Possible Role of the Interactions between the N- and C-Termini To Maintain the Inhibitory Active Form of Cystatin A[†,‡]

Shin-ichi Tate,[§] Toshio Ushioda,[||] Naoko Utsunomiya-Tate,[§,⊥] Kazunori Shibuya,[||] Yukihito Ohyama,[||] Yasuhiro Nakano,[§] Hiroyuki Kaji,[§,||] Fuyuhiko Inagaki,[#] Tatsuya Samejima,[||] and Masatsune Kainosho*[,§]

Department of Chemistry, Faculty of Science, Tokyo Metropolitan University, 1-1 Minamiohsawa, Hachioji, Tokyo, 192-03 Japan, Department of Chemistry, College of Science and Engineering, Aoyama Gakuin University, 6-161-1 Chitosedai, Setagaya-ku, Tokyo, 157 Japan, School of Medicine, Kyorin University, 6-20-2 Shinkawa, Mitaka, Tokyo, 181 Japan, and Department of Molecular Physiology, Tokyo Metropolitan Institute of Medical Science, 3-18-22 Honkomagome, Bunkyo-ku, Tokyo, 113 Japan

Received July 5, 1995; Revised Manuscript Received August 28, 1995[⊗]

ABSTRACT: The solution structure of a human cystatin A variant, cystatin A^{2-98} M65L, which maintains the full inhibitory activity of the wild-type protein, was determined at pH 3.8 by 2D/3D heteronuclear double- and triple-resonance NMR spectroscopy. The structure is based on a total of 1343 experimental restraints, comprising 1139 distance, 154 ϕ and χ^1 torsion angle restraints, and 50 distance constraints for 25 backbone hydrogen bonds. A total of 15 structures was calculated using the YASAP protocol with X-PLOR, and the atomic rms distribution about the mean coordinate positions for residues 8−93 was 0.55 ± 0.10 Å for the backbone atoms and 1.05 ± 0.11 Å for all heavy atoms. The structure consists of five antiparallel β-sheets and two short α-helices. Comparison with the X-ray structure of cystatin B in the papain complex shows that the conformation of the first binding loop is quite similar to that of cystatin A, with an rms deviation of 0.78 Å for the backbone atoms in the 43−53 region (cystatin A numbering). The second binding loop, however, is significantly different in the two structures, with an rms deviation greater than 2 Å. There are some other significant differences, especially for the N-terminal and α-helix regions. The overall structure of cystatin A is also compared with the recently reported NMR structure of the wild-type cystatin A (stefin A) at pH 5.5 (Martin et al., 1995) and reveals the following features that differ in our structure from the previous one: (1) the N-terminal segment, which was unstructured in the previous report, folds over in close vicinity to the C-terminus, as revealed by the distinctive NOEs between those segments; (2) two discrete short α-helices linked by a type II reverse turn were found, instead of the continuous single α-helix with a slight kink shown in the previous structure; (3) the second binding loop, which was not well converged in the previous study at pH 5.5, is determined very well in our structure. The effect of the N-terminal truncation on the cystatin A structure was examined by comparing the $^1H-^{15}N$ HSQC spectrum of cystatin A^{2-98} with that of the cystatin A^{5-98} variant, which lacks the anti-papain activity, revealing significant chemical shift differences in the residual N-terminal segment and the first binding loop, together with small shifts in the other parts. The results imply that the conformational changes in the first binding loop, induced by the N-terminal truncation, are responsible for the loss of inhibitory activity. A possible role of the N- and C-interterminal interactions in maintaining the active conformation of cystatin A is discussed.

Cysteine proteinase inhibitors are widely distributed in mammals, plants, and insects and may function to protect cells from unwanted proteolysis and to control intra- or extracellular protein breakdown (Barrett, 1987). The cystatin superfamily, which consists of sequentially homologous inhibitors with tight, but reversible, binding properties (Barrett et al., 1986), has been further classified into three subfamilies, namely, type 1 (stefin family), lacking disulfide bridges, type 2 (cystatin family), with two disulfide bridges, and type 3 (kininogen family), which actually consists of three type 2-like domains (Turk & Bode, 1991). The crystal structures have been determined for the Gly form of chicken cystatin (Bode et al., 1988), a type 2 inhibitor, lacking the first eight N-terminal residues, and for cystatin B (stefin B), a type 1 inhibitor, as the papain complex (Stubbs et al., 1990). Recently, the solution structures of native phosphorylated and recombinant unphosphorylated chicken cystatins were determined by NMR (Dieckmann et al., 1993). The solution and crystal structures of the chicken cystatins were compared

[†] This work is supported in part by a Grant-in-Aid for Priority Areas (No. 05244101) and a Grant-in-Aid for Specially Promoted Research (No. 05101004) from the Ministry of Education, Science and Culture, Japan, and by the special coordination fund of the Science and Technology Agency. S.T. acknowledges support from the Nestlé Science Promotion Committee. A portion of this work was presented at the 16th International Conference on Magnetic Resonance in Biological Systems, Aug 14−19, 1994, Veldhoven, The Netherlands.

[‡] Coordinates have been deposited in the Brookhaven Protein Data Bank under the file name Cystatin A 1CYU and 1CYV.

* To whom correspondence should be addressed: telephone, +81-426-77-2544; Fax, +81-426-77-2525; E-mail, kainosho@raphael.chem.metro-u.ac.jp.

[§] Tokyo Metropolitan University.

[||] Aoyama Gakuin University.

[⊥] Kyorin University.

[#] Tokyo Metropolitan Institute of Medical Science.

[⊗] Abstract published in *Advance ACS Abstracts,* October 15, 1995.

0006-2960/95/0434-14637$09.00/0

to each other and also to the crystal structure of cystatin B in the papain complex (Engh et al., 1993). On the basis of the crystal structure of chicken cystatin, the mode of the interaction with the cognate proteinase has been predicted (Machleidt et al., 1989; Bode et al., 1988). In the model, the first and the second binding loops, together with the N-terminus, form a hydrophobic wedge-shaped "edge", which is highly complementary to the active site cleft of papain. This interaction mode was subsequently proven by the X-ray analysis of the human cystatin B−papain complex (Stubbs et al., 1990).

It should be pointed out, however, that the N-terminal truncated cystatin B, cystatin B^{7-98}, maintained full anti-papain activity, indicating that the interactions between the N-terminal segment of the intact cystatin B and papain are *not* essential for the inhibitory activity (Thiele et al., 1990), even though an elegant model, based on the crystal structure of chicken cystatin, has been proposed for the molecular recognition processes between papain and cystatin (Machleidt et al., 1989; Bode et al., 1990). Abe et al. (1988) reported that oryzacystatin, another type 1 inhibitor, like cystatin B, showed no activity loss by truncation of the N-terminal 21 residues and concluded that the N-terminal segment is not essential for the anti-papain activity. In the case of chicken cystatin, a type 2 inhibitor, however, the N-terminal truncation including Gly^9, which corresponds to the highly conserved Gly^4 in cystatins A and B, completely abolished its inhibitory activity (Machleidt et al. 1989; Bode et al., 1988; Abrahamson et al., 1987). It is important to realize that the Gly form of chicken cystatin, for which the X-ray structure has been reported, lacks inhibitory activity (Bode et al., 1988). Intriguingly, the N-terminal truncation experiments of cystatin A, a type 1 cystatin sharing 54% sequence homology with cystatin B, showed that the activity was completely lost by removing a segment of the N-terminal residues including the conserved Gly^4 (cystatin A and B numbering) (Shibuya et al., 1995a). The explanation for differential effects of the N-terminal truncations among the cystatins is one of the most important issues yet to be resolved.

On the other hand, the major role of the first binding loops with the highly conserved QVVAG sequence (from Gln^{46} to Gly^{50} in cystatin A numbering) in the inhibitory activity has been well established. In the crystal structure of the cystatin B−papain complex, many close intermolecular contacts of less than 4 Å have been found for the first binding loops, while the fewer close intermolecular contacts for the second binding loop of cystatin B show that it might have only secondary importance in proteinase binding. The role of the conserved region in the first binding loop has been extensively studied by site-directed mutagenesis (Nikawa et al., 1989; Jerala et al., 1990; Arai et al., 1991; Auerswald et al., 1992). Single amino acid substitutions of the QVVAG sequence in most cases result in a drastic reduction in papain inhibition (Machleidt et al., 1991; Arai et al., 1991; Auerswald et al., 1992). There are, however, some examples showing that the mutations in the first binding loop in the cystatins do not change their inhibitory activities (Nikawa et al., 1989; Jerala et al., 1990). These apparently contradictory results obtained for the cystatin superfamily inhibitors should be explained eventually by a unified structural basis, rather than by sequence comparisons and mutagenesis. As a first step to this ultimate goal, we have investigated the molecular details of the inactivation process of cystatin A, induced by the N-terminal truncation, by NMR spectroscopy.

Cystatin A, which is an acidic protein (p*I* 4.5) belonging to the cystatin superfamily, has been isolated from human polymorphonuclear granulocytes (Brzin et al., 1982), spleen (Brzin et al., 1983), liver (Green et al., 1984), and epidermis (Järvinen, 1978). The amino acid sequence of cystatin A, isolated from human leukocytes (Brzin et al., 1983), has been determined by Machleidt et al. (1983). An overexpression system for cystatin A in *Escherichia coli* has been constructed as a fusion protein with porcine adenylate kinase, using a chemically synthesized human cystatin A gene (Kaji et al., 1989). The cystatin A gene contains one amino acid replacement, M65L, to facilitate the BrCN cleavage procedure used to isolate the recombinant cystatin A from the fused protein (Kaji et al., 1989). The isolated cystatin A, which is actually the cystatin A^{2-98} M65L variant, since Met^1 is lost in the BrCN treatment, exhibits the same level of inhibitory activity as the wild-type cystatin A (Kaji et al., 1989). We denote this cystatin A variant as cystatin A hereafter. We have prepared uniformly ^{15}N- and $^{15}N/^{13}C$-labeled cystatin A and some selectively labeled cystatin A proteins, which made it possible to use various triple-resonance heteronuclear 2D- and 3D-NMR methods to determine a well-defined solution structure at pH 3.8. After the completion of our work, the solution structure of the wild-type cystatin A at pH 5.5 was published by Martin et al. (1995). We compare the two cystatin A structures determined under different solution conditions and correlate their differences with the crystal structure of cystatin B in the papain complex (Stubbs et al., 1990).

EXPERIMENTAL PROCEDURES

Sample Preparation. Expression and purification of cystatin A from an *E. coli* culture were carried out according to the protocol previously described (Kaji et al., 1989). Uniformly $^{15}N/^{13}C$-labeled cystatin A was produced using essentially the same conditions, but in M9 medium containing [^{13}C]glucose (99% ^{13}C; Shoko Co. Ltd., Tokyo) and [^{15}N]-ammonium chloride (99% ^{15}N; Shoko Co. Ltd., Tokyo) as the sole carbon and nitrogen sources. The *E. coli* NM522 strain was used in lieu of the JM109 strain in the original protocol, since this strain produced more cystatin A in the M9 medium. The cystatin A proteins containing either the "block" ^{13}C-labeled Val or Leu were prepared by adding either of these "block" ^{13}C-labeled amino acids into the M9 medium (see below). The variant lacking the four residues at the N-terminus, cystatin A^{5-98} M65L, was prepared by the same protocol as described above, using *E. coli* harboring the truncated cystatin A gene (Shibuya et al., 1995). The lyophilized proteins were dissolved in either 95% H_2O/5% D_2O or 99% D_2O at pH 3.8 (direct meter reading). For NMR measurements, 220 μL of the solution (1.0−1.5 mM) was placed into a Shigemi microcell (Shigemi Co., Ltd., Tokyo).

NMR Spectroscopy. 3D HNCA and 3D HNCO spectra (Kay et al., 1990) with gradient sensitivity enhancement were acquired as described by Muhandiram and Kay (1994) on a UNITY plus-500 spectrometer. 3D CBCA(CO)NH and CBCANH spectra were recorded in a gradient sensitivity enhancement manner (Muhandiram & Kay, 1994; Grzesiek & Bax, 1992a,b). 3D ^{15}N-edited TOCSY-HSQC and NOESY-HSQC spectra (Marion et al., 1989a,b; Driscoll et al., 1990; Fesik & Zuiderweg, 1990) were collected using a gradient sensitivity enhancement procedure (Kay et al., 1992) in the HSQC portion of these pulse sequences. The Z-axis isotropic mixing, of 45 ms duration, with DIPSI-2 (Shaka et al., 1985)

was used in the TOCSY-HSQC. NOESY-HSQC data were acquired using mixing times of 75, 100, and 150 ms.

The 3D ^{13}C-edited NOESY-CT-HSQC experiment (Vuister & Bax, 1992) was carried out on an AMX 500 spectrometer. The total CT duration was set to 6.6 ms. The NOESY mixing time was set to 75 ms. 3D HCCH-TOCSY (Bax et al., 1990a) and HCCH-COSY (Bax et al., 1990b) were carried out with the parameters described in the literature. For the ^{13}C isotropic mixing in HCCH-TOCSY with 22.8 ms duration, the DIPSI-2 (Shaka et al., 1988) sequence was used at a 7.5 kHz field strength. 3D HNHB (Archer et al., 1991) and HNHA data (Vuister & Bax, 1993) were also acquired in order to obtain the $^3J_{NH\beta}$ and $^3J_{HN-H\alpha}$, respectively. 3D CT-HCCH-E.COSY (Griesinger & Eggenberger, 1992; Eggenberger et al., 1992) was used to estimate $^3J_{H\alpha-H\beta}$. The experimental conditions were as described in the literature, except for the pulsed field gradient used in our experiments.

The acquired data were processed with either FELIX (Biosym Technologies, Inc., San Diego) or nmrPipe/nmrDraw (Delaglio, NIH). Peak picking in the 3D data and peak intensity estimation of the picked cross peaks were carried out by PIPP (Garrett et al., 1991). The NOESY peak assignments were made using the PIPP/CAPP/STAPP software package (Garrett, NIH) on the NMR data processed with nmrPipe. The data processing with FELIX was carried out on an INDIGO/Elan workstation (Silicon Graphics), and all data processing and spectral analysis using nmrPipe/nmrDraw and PIPP/CAPP/STAPP were done on either Sun Sparc 10 or Sun Sparc 20 workstations.

NOE Distance Constraints. Interproton distance restraints were derived from the NOEs assigned in the 3D ^{15}N-edited NOESY-HSQC spectrum with the 100 ms mixing time and the 3D ^{13}C-edited NOESY-CT-HSQC spectrum with the 75 ms mixing time. The 3D ^{1}H$-^{15}$N NOESY-HSQC spectra with mixing times of 75 and 150 ms were used as supplements in this step. The assigned NOEs were classified into upper bound distance restraints of 2.8, 3.5, 5.0, and 6.0 Å, respectively. The lower bounds for the interproton distance restraints were set to the sum of the van der Waals radii of two protons. Upper distance limits for the distances involving methyl protons and nonstereospecifically assigned methyl protons were corrected appropriately for center averaging (Wüthrich et al., 1983), and an additional 0.5 Å was added to the upper distance limits for the NOEs involving methyl protons (Clore et al., 1987; Wagner et al., 1987).

Stereospecific Assignment of β-Methylene and χ^1 Restraints. Stereospecific assignments of the β-methylene protons and the χ^1 angle restraints were derived from the interproton distances obtained from the 3D ^{15}N-edited NOESY with 75 ms mixing and the 3D ^{13}C-edited NOESY with 75 ms mixing, together with the J coupling constants obtained from the 3D HNHB for $^3J_{N-H\beta}$ and the 3D HCCH-E.COSY for $^3J_{H\alpha-H\beta}$. On the basis of the experimentally estimated χ^1 rotamer, the χ^1 angle restraints were determined as 180, −60, and 60, with allowed ranges of ±30° or ±60°. The ϕ angle restraints were derived from the 3D HNHA spectrum; on the basis of the observed magnitude of $^3J_{NH-H\alpha}$, the ϕ angle was restrained to be −120° and −60° with one of the three angle ranges: ±30°, ±40°, or ±60°.

Hydrogen-Bonding Restraints. Hydrogen-bonding restraints were identified with the evidence of the slow amide proton−solvent exchange rate monitored in a series of 2D ^{1}H$-^{15}$N HSQC spectra of lyophilized protein freshly dissolved in D_2O, which was recorded with the combined use of water flip-back (Grzesiek & Bax, 1993) and WATERGATE (Piatto et al., 1992) solvent suppression. The first HSQC experiment was started within 20 min after the addition of D_2O. Each identified bond was defined using two distance restraints: r_{NH-O} = 1.5−2.5 Å and r_{N-O} = 2.5−3.5 Å.

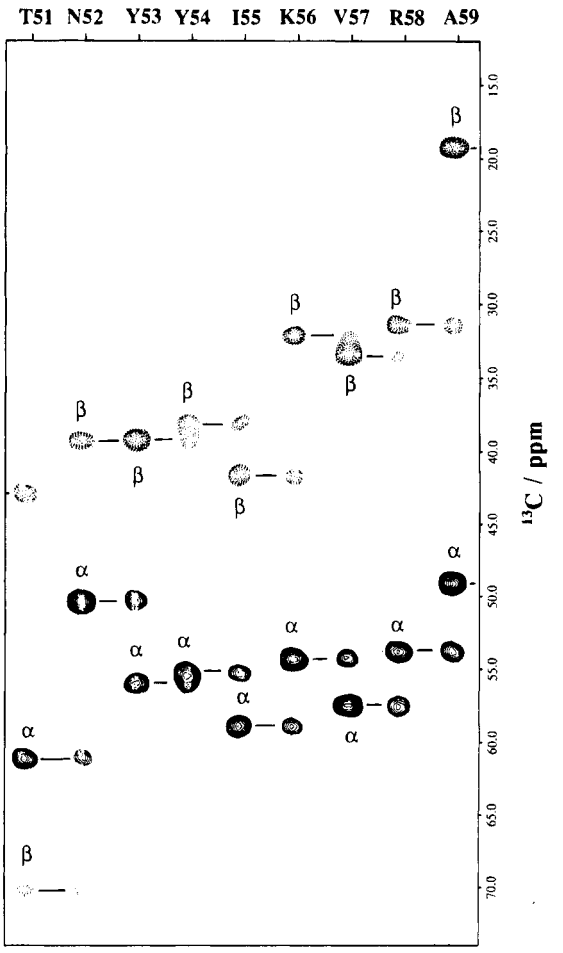

FIGURE 1: Sequential strips extracted from the CBCANH experiment. Intraresidue correlations are labeled with Greek symbols.

Structure Calculations. Structures were generated using the YASAP protocol (Nilges et al., 1988, 1991) within the X-PLOR 3.1 program (Brünger, 1992). In progressing the NOE assignments to increase the number of incorporated distance restraints, we employed an interactive refinement strategy using the efficient assignment tool PIPP (Garrett et al., 1991), essentially according to the process described by Powers et al. (1993). Finally, 1343 experimental NMR restraints were incorporated into the calculation: 1139 approximate interproton distance restraints, 50 distance restraints for 25 backbone hydrogen bonds, and 154 torsion angle restraints for ϕ and χ^1. All structure calculations with X-PLOR were performed on the Silicon Graphics INDIGO/Elan workstation. For the graphical presentation of the observed results, and the structure comparison displays, the Insight II program (Biosym Technologies Inc., San Diego) was used on the INDIGO/Elan workstation.

RESULTS

Resonance Assignments. The assignments of the main-chain NH, ^{15}N, $^{13}C^{\alpha}$, and $^{13}C^{\beta}$ NMR signals were made using the 3D CBCA(CO)NH and CBCANH spectra together with the 3D HNCA spectrum. Figure 1 shows an example of the sequential strips, extracted from the CBCANH experi-

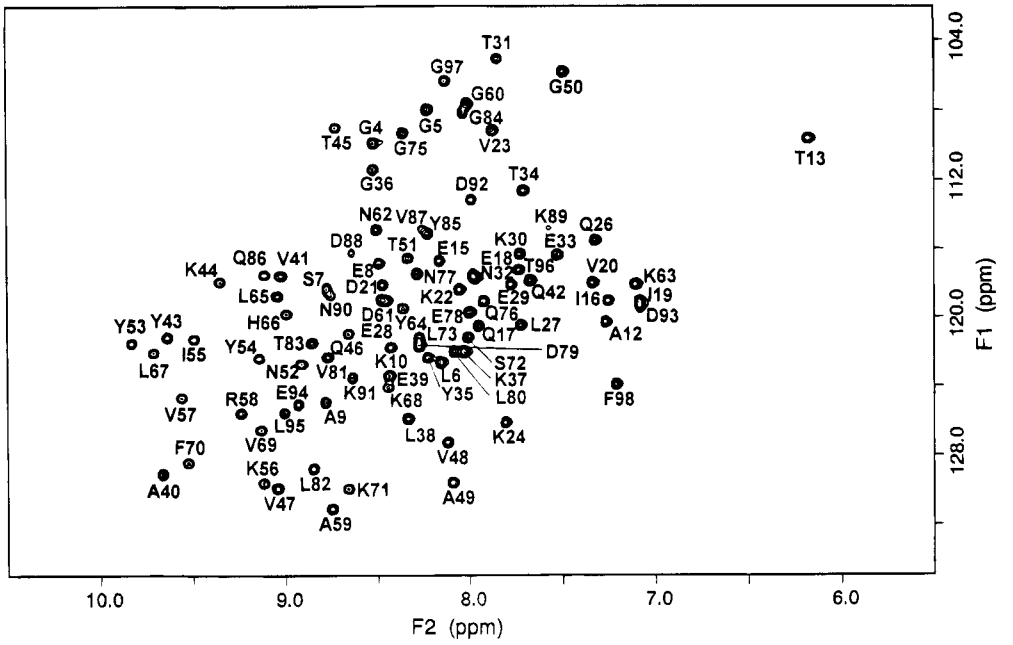

FIGURE 2: $^{1}H-^{15}N$ HSQC spectrum of uniformly ^{15}N-labeled cystatin A. The side-chain amide protons are suppressed by the application of refocus INEPT transfers and synchronous ^{1}H decoupling with WALTZ-16 during the ^{15}N t_1 evolution period. The assignments obtained in the present study are indicated.

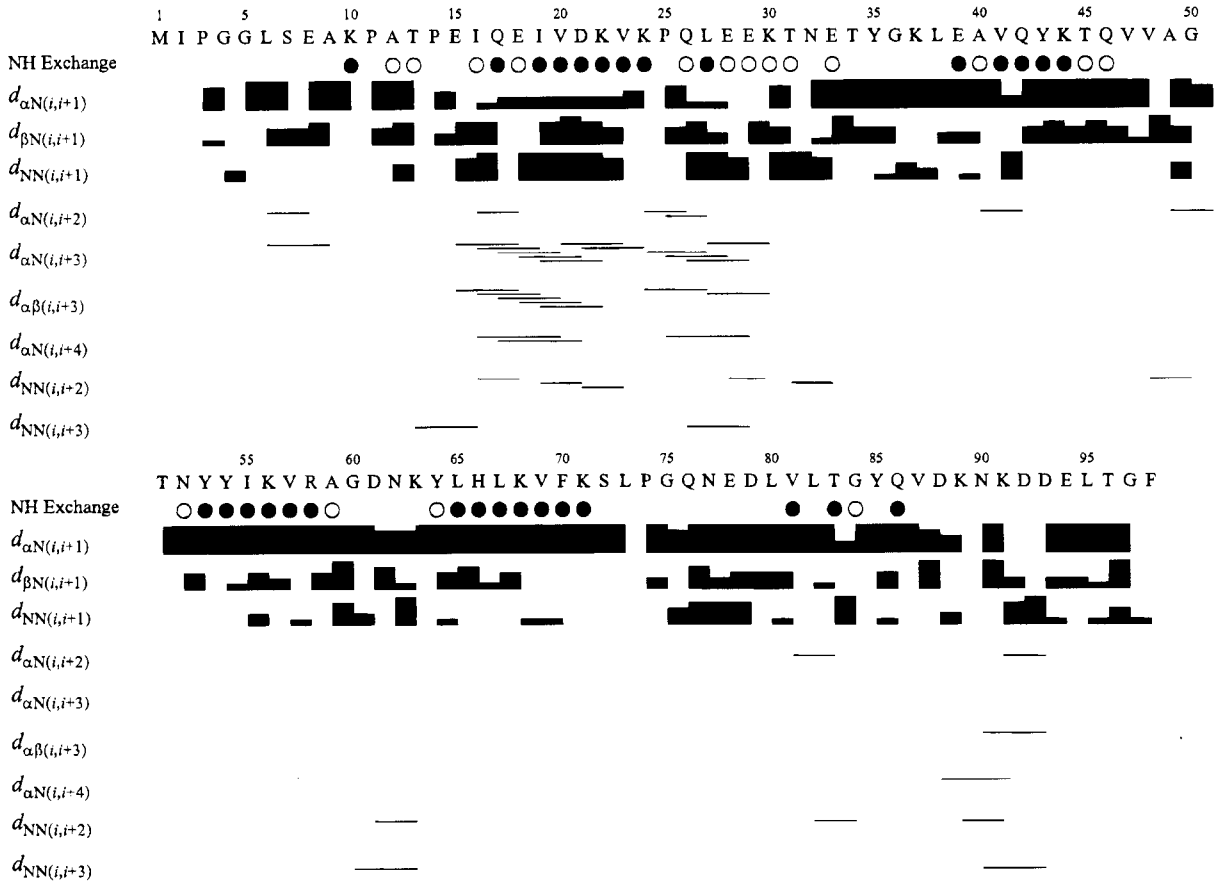

FIGURE 3: Diagram of short-range NOE connectivities for cystatin A. The NOE correlations were determined from the 3D NOESY spectra recorded at 37 °C. The height of the bar indicates the strength of the NOE correlation. Filled circles indicate residues with amide ^{1}H resonances that are not fully exchanged within 2 h in the $^{1}H-^{15}N$ HSQC experiment after the lyophilized sample was dissolved in the D_2O solution.

ment, ranging from Thr[51] to Ala[59]. The carbonyl carbon assignment was obtained by the 3D HNCO experiment. The assignments for the side-chain ^{1}H signals were obtained from the 3D HCCH-TOCSY and 3D HCCH-COSY spectra on the basis of the main-chain signal assignment described above. A selected plane of the 3D HCCH-TOCSY spectrum is shown in Figure S-1 (see supporting information). From the above spectral analysis, we could assign all of the ^{1}H, ^{15}N, $^{13}C^{\alpha}$, $^{13}C^{\beta}$, and $^{13}C'$ signals. A list of all of the assigned chemical shifts of cystatin A is attached as supporting information (Table S-1a,b). The assignments of the backbone ^{1}H and ^{15}N signals are shown on the 2D HSQC

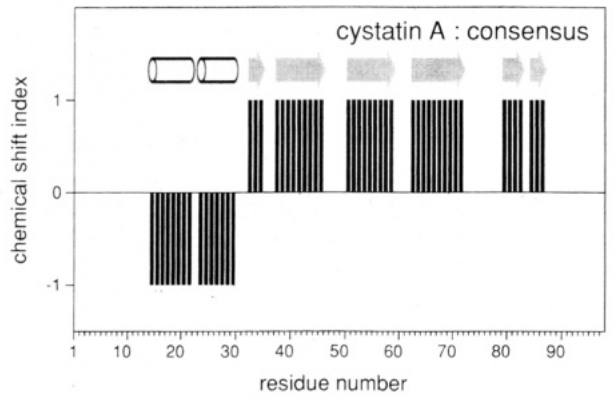

FIGURE 4: "Consensus map" of the chemical shift index profile for cystatin A, calculated by the program CSI (Wishart & Sykes, 1994).

spectrum with the suppressing side-chain NH_2 signals of Gln and Asn (Bax et al., 1990c) in Figure 2.

Secondary Structure. The NOE connectivities of cystatin A are summarized in Figure 3, along with the locations of the slowly exchanging amide protons. For this analysis, the 3D ^{15}N-edited NOESY-HSQC with a mixing time of 150 ms and the 3D ^{13}C-edited NOESY-CT-HSQC with a 75 ms mixing time were used. Two selected planes of the 3D ^{13}C-edited NOESY-CT-HSQC spectrum are shown in Figure S-2. The $d_{\alpha\beta}(i,i+3)$ and $d_{\alpha N}(i,i+3)$ connectivities typically found in the α-helix portion are broken at Lys^{22}, and they begin again at Lys^{24}. From the chemical shift index analysis (Wishart & Sykes, 1994), the C^{α} and H^{α} chemical shifts of Val^{23} have opposite signs of the indices from those for an α-helix, implying that Val^{23} is not in an α-helix (Figure S-3a,b). From this evidence, it is clear that the regions from Glu^{15} to Lys^{22} and from Gln^{26} to Lys^{30} form two distinct, short α-helices. The NOE connectivities observed among residues Lys^{24}−Leu^{27}, however, deviate from a typical α-helix pattern. The intense $d_{\alpha N}(i,i+1)$ connectivity observed for Pro^{25} and Glu^{26}, together with the $d_{\alpha N}(i,i+2)$ connectivity found for Pro^{25} and Leu^{27}, strongly indicates that these four residues form a type II turn (Wüthrich, 1986), which links the two short α-helices. Three β-bulges are found in cystatin A, at Val^{41}, Thr^{83}, and Asp^{88}, which are typically identified from the observation of the small $d_{\alpha N}(i,i+1)$ and large $d_{NN}(i,i+1)$ connectivities within the β-sheet portion. A schematic representation of the secondary structure deduced from the NOE patterns is shown in Figure 5. The NOE-based analysis was 88%, consistent with the chemical shift index analysis on the "consensus" map (Figure 4). The other chemical shift index maps can be found in supporting information (Figure S-3a−d).

Stereospecific Assignments of the Valyl and Leucyl Methyl Groups. Stereospecific assignments of the diastereotopic methyl groups of the Val and Leu residues have been established by the ^{1}H−^{13}C CT-HSQC spectra, with total CT durations of 14.3 and 28.6 ms, for the cystatin A proteins labeled selectively with either the "block" ^{13}C-labeled Val or Leu. With a CT duration of 28.6 ms, the *pro-R* methyls, each of which has a 35 Hz ^{13}C−^{13}C spin coupling with a directly bonded carbon, and the *pro-S* methyls, which lack such coupling, show opposite signs, and only the *pro-S* methyls are observed with a 14.3 ms duration. The assignments are listed in Table 1. The block ^{13}C-labeled Val and Leu stand for the fractional ^{13}C-labeled Val and Leu prepared by the microbial fermentation, using a mixture of 98% ^{13}C

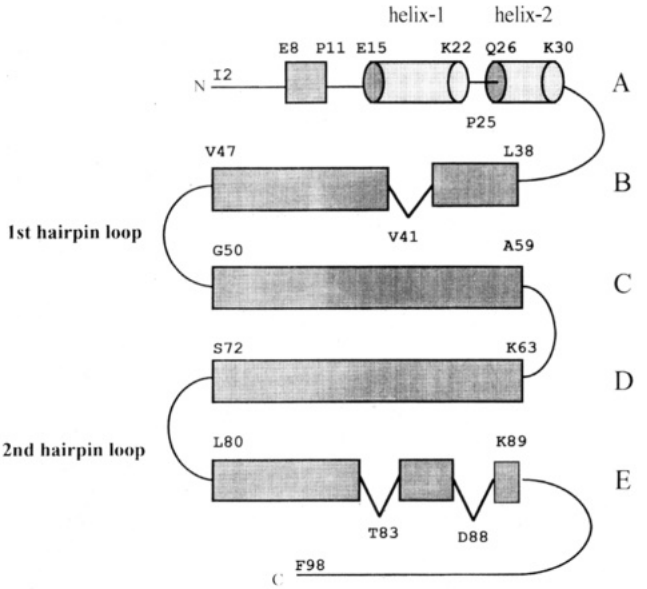

FIGURE 5: Schematic representation of the secondary structure of cystatin A. Rectangular boxes represent β-sheets and cylinders represent helices. The five β-strands are denoted as A−E (shown in the right) and the two α-helices as helix 1 and helix 2 (shown at each helix).

Table 1: Stereospecific Assignment and ^{13}C and ^{1}H Chemical Shifts (ppm) of Diastereotopic Methyls of Valyl and Leucyl Residues in Cystatin A

residues		^{13}C	^{1}H	residues		^{13}C	^{1}H
Leu^{6}	δ1[a]	22.9	0.49	Val^{20}	γ1[a]	20.9	0.69
	δ2[a]	24.0	0.20		γ2[a]	24.1	0.84
Leu^{27}	δ1	21.0	0.20	Val^{23}	γ1	19.6	0.85
	δ2	25.3	0.25		γ2	17.7	0.93
Leu^{38}	δ1	24.5	0.55	Val^{41}	γ1	20.0	1.11
	δ2	22.7	0.49		γ2	19.5	1.11
Leu^{65}	δ1	24.5	0.55	Val^{47}	γ1	20.0	1.06
	δ2	26.1	0.79		γ2	19.8	0.97
Leu^{67}	δ1	24.7	0.70	Val^{48}	γ1	21.0	0.79
	δ2	22.6	0.83		γ2	17.8	0.70
Leu^{73}	δ1	23.8	0.87	Val^{57}	γ1	21.1	0.73
	δ2	21.2	0.91		γ2	20.6	0.79
Leu^{80}	δ1	25.3	0.80	Val^{69}	γ1	22.1	0.70
	δ2	22.9	0.73		γ2	20.9	0.77
Leu^{82}	δ1	25.3	0.79	Val^{81}	γ1	20.1	0.92
	δ2	25.6	0.75		γ2	19.5	1.00
Leu^{95}	δ1	23.6	0.64	Val^{87}	γ1	20.0	1.08
	δ2	21.5	0.32		γ2	16.9	0.90

[a] γ1, δ1 and γ2, δ2 correspond to the *pro-R* and the *pro-S* methyls, respecively.

[$^{13}C_6$]glucose and unlabeled glucose at 15% and 85%, respectively, as the sole carbon source. The ^{13}C distributions of the obtained Val and Leu reflect the mechanism as well as the stereochemistry of the biosynthetic pathways of each amino acid, which are well established for Val and Leu (Sylvester & Stevens, 1979, and references cited therein). A detailed account of the preparation of the block ^{13}C-labeled amino acids and their use in protein NMR will be described elsewhere (Kainosho et al., in preparation). A similar idea has been described by Neri et al. (1989) and was referred to as "biosynthetically directed fractional ^{13}C-labeling". In their approach, protein synthesis is carried out using a mixture of 98% ^{13}C [$^{13}C_6$]glucose and unlabeled glucose, and therefore, all of the amino acids of the protein are labeled simultaneously.

Structure Determination. A total of 1343 experimental restraints was used in the structure calculation with X-PLOR.

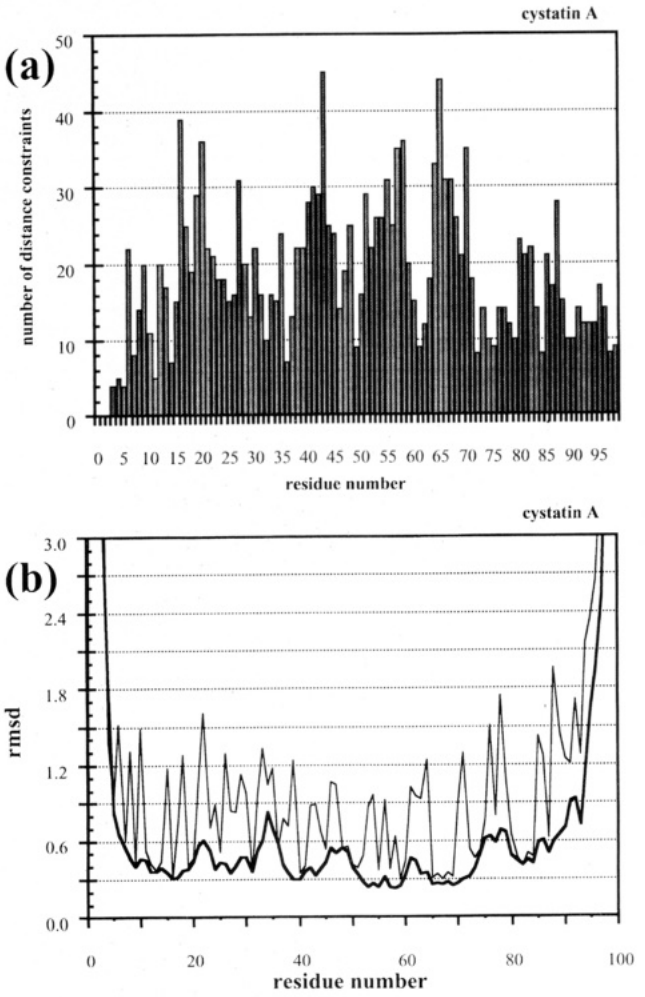

FIGURE 6: (a) Distribution of the number of distance constraints on the primary sequence of cystatin A. (b) Plots of residue-specific rms displacements for the 15 refined NMR structures. The heavy trace shows the average backbone atom rmsd for each residue between the 15 refined coordinates and the mean structure, after global fitting of the backbone atoms. The thinner trace shows the corresponding data for the side-chain heavy atoms.

The distribution of the distance constraints against the primary sequence of cystatin A is plotted in Figure 6a. Structural statistics for the final converged 15 structures of cystatin A are summarized in Table 2, and the best-fit superposition of the backbone atoms about the mean coordinate is shown in Figure 7. The structures satisfy the experimental restraints well (Table 2); there are no interproton distances and torsion angle violations greater than 0.5 Å and 5°, respectively, in these refined structures. The atomic rms deviations for the backbone and heavy atoms are plotted on a per residue basis in Figure 6b. The atomic rms deviations of this ensemble of refined structures were estimated in two ways on different ranges of sequences; the rms deviations, pairwise and against the mean coordinate, were estimated for all residues of cystatin A and also for all residues, except the less defined N- and C-terminal segments (Table 3). A Ramachandran plot for the final converged 15 structures is available in supporting materials (Figure S-4).

Table 2: Structural Statistics

	15 structures	mean structure
rmsd from exptl distance constraints (Å)		
all (1189)	0.054 ± 0.001	0.05
intraresidual (451)	0.033 ± 0.002	0.033
sequential[a] (319)	0.066 ± 0.002	0.067
medium range[b] (132)	0.064 ± 0.004	0.064
long range[c] (237)	0.061 ± 0.003	0.058
H-bond (50)	0.052 ± 0.003	0.052
rmsd from exptl dihedral angle constraints (deg) (154)	0.41 ± 0.06	0.36
rmsd from idealized geometry		
bonds (Å)	0.0048 ± 0.0001	0.0047
angles (deg)	0.7748 ± 0.0101	0.7653
impropers (deg)	0.5328 ± 0.0110	0.5194

[a] $|i-j|=1$. [b] $|i-j|\leq 5$. [c] $|i-j|>5$.

Table 3: Atomic rms Deviations

	backbone atoms	all heavy atoms
all residues (2 − 98)		
pairwise (Å)	1.35 ± 0.53	1.84 ± 0.46
against mean structure (Å)	1.14 ± 0.28	1.73 ± 0.25
internal residues (8 − 93)		
pairwise (Å)	0.55 ± 0.13	1.12 ± 0.14
against mean structure (Å)	0.55 ± 0.10	1.05 ± 0.11

pH Dependency of the Amide Protons and Nitrogens. The $^{1}H-^{15}N$ HSQC spectra of cystatin A have been measured in

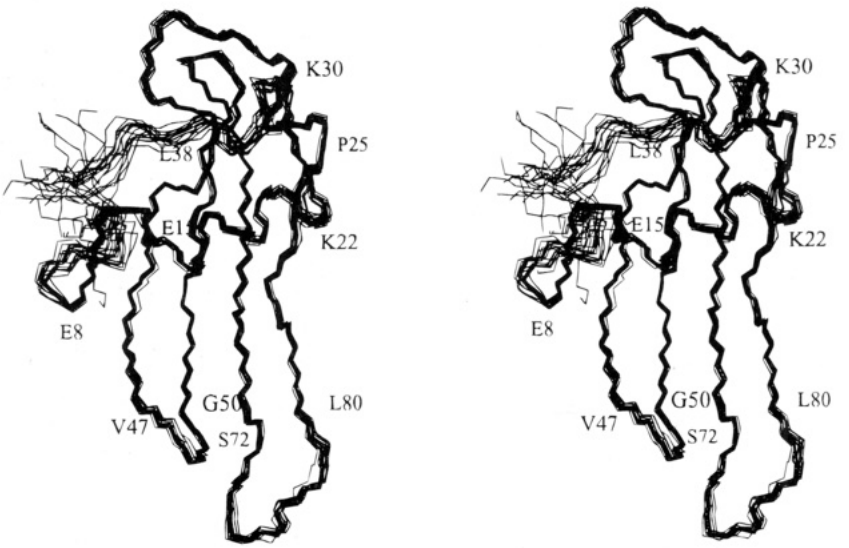

FIGURE 7: Stereopairs of the best-fit superposition of the 15 final converged structures of cystatin A. The backbone atoms (N, C^{α}, and C′) are displayed. The calculation of the best-fit superposition and their display were carried out with Insight II version 2.2.0 (Biosym Technologies, Inc., San Diego).

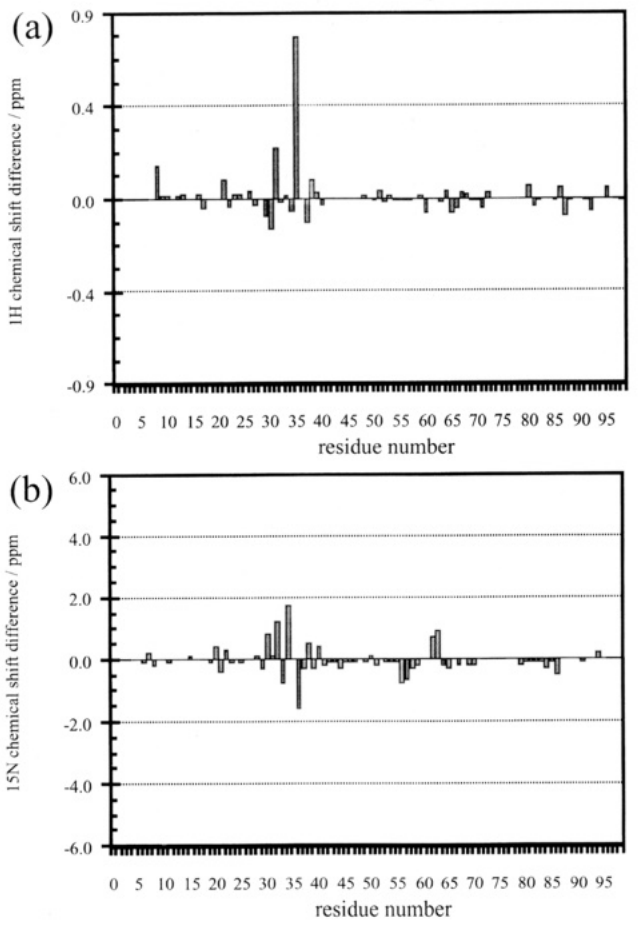

FIGURE 8: Changes in chemical shifts observed during the pH titration for the amide protons (a) and the amide nitrogens (b). Each bar represents the difference between the assigned chemical shift at pH 3.8 and 7.2 for the amide in the corresponding sequence position.

the pH range 3.8−7.1 in order to detect any possible structural changes that might occur at lower pHs. The chemical shift changes are summarized in Figure 8 and show that there are notable changes for very limited regions: the amide protons of Thr^{31} and Tyr^{35} move by greater than 0.2 ppm, and the amide nitrogens of Glu^{33}, Tyr^{35}, and Lys^{37} move by more than 1.0 ppm between pH 3.8 and pH 7.1. As can be seen from an overlay of the $^1H-^{15}N$ HSQC spectra observed at different pHs, which is shown in Figure S-5 in supporting information, the rest of the spectra are almost unchanged over this pH range. The residues that show large chemical shift changes are confined to those located near the surface in the large loop region, which links the α-helices to the second β-strand. This observation shows that the overall structure of cystatin A does not change between acidic and neutral pHs. By measuring the NMR spectra at pH 3.8, which is close to the pH where the backbone amide protons show minimal exchange rates (Wüthrich, 1986), we could observe many NOEs derived from the relatively fast exchanging amide protons, which may be overlooked at higher pHs.

Effect of the N-Terminal Truncation on the Conformations and the Binding Activity of Cystatin A. Shibuya et al. recently found that a cystatin A variant missing the first four N-terminal residues lacks papain binding activity (Shibuya et al., 1995a). In order to clarify the possible origins of the drastic effect of this N-terminal truncation, we have investigated the effect of the truncation on the overall structure of cystatin A. We thus compared the $^1H-^{15}N$ HSQC spectra

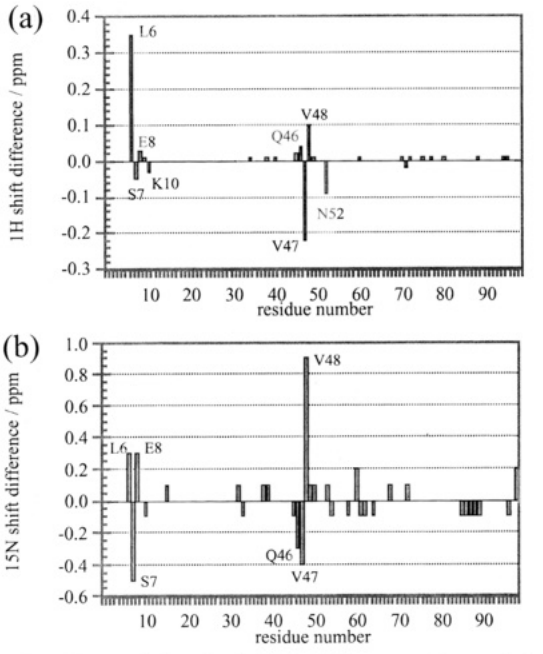

FIGURE 9: Plots of chemical shift differences observed in the comparison of the spectra of cystatin A and cystatin A^{5-98}; δ(cystatin A^{5-98}) − δ(cystatin A) is plotted for each residue. The chemical shift differences observed in the ^1H dimension (a) and the ^{15}N dimension (b) are shown in different panels.

of cystatin A and cystatin A^{5-98}. As shown in Figure 9, in addition to the NMR signals due to the N-terminal residues Leu^6, Ser^7, and Glu^8, the signals belonging to Gln^{46}, Val^{47}, and Val^{48}, which are far from the N-terminus in the sequence, showed substantial chemical shift changes. All of these residues are in the first hairpin loop, which comprises the highly conserved QVVAG sequence. Small chemical shift changes are also observed in such regions as strands A−C and the C-terminal segment. The rest of the signals are almost unchanged, indicating that the structural changes are limited to the N-terminal segment, the first binding loop and its vicinity, and the C-terminal segment.

DISCUSSION

Structural Comparison of Cystatin A with Cystatin B in the Papain Complex and with Solution and Crystal Structures of Other Cystatins. (A) The α-Helix Region. The average solution structure of cystatin A, generated from the 15 refined coordinates, is shown by an overlay with the X-ray structure of cystatin B in the papain complex (Stubbs et al., 1990; PDB accession code 1STF) (Figure 10). In this presentation, the β-sheet portions, consisting of strands B−E (residues Leu^{38} −Lys^{89}), are maximally overlapped. Although cystatins A and B share 54% sequence homology, some notable structural variations exist. A significant difference was found in the α-helix portion, as expected. Among all the cystatins, cystatin A is unique in that it has proline, Pro^{25}, in the middle of the α-helix portion that has been identified for cystatin B (Stubbs et al., 1990). In cystatin B, the α-helix is a single, continuous structure with a very slight kink at Ser^{25}, indicating that the helix might have a tendency to bend at this position, even without proline. It would therefore be rather surprising if proline, which is well recognized as a helix breaker (Chou & Fasman, 1978), at this position did not alter the α-helix conformation. We actually found that the helix portion did break into two short, but distinct α-helices exactly at Pro^{25}. As discussed previously, the NOE

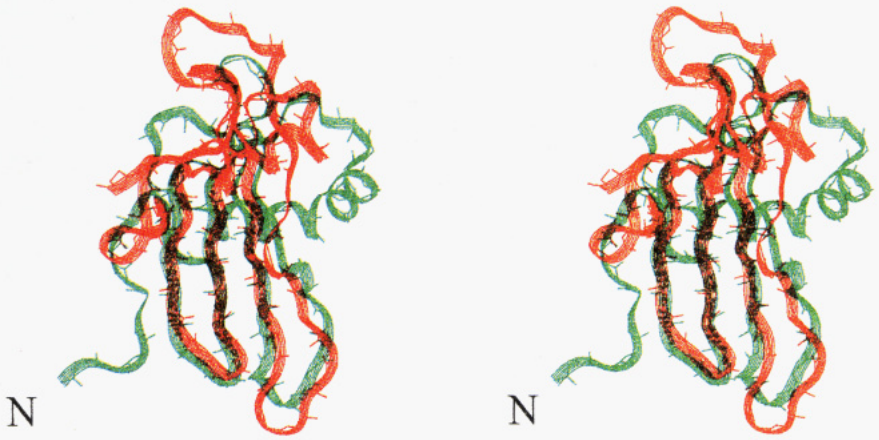

FIGURE 10: Comparison of the mean coordinate calculated from the 15 final converged structures of cystatin A (red ribbon) and the crystal structure of cystatin B in a complex with papain (green ribbon), shown by the superposition of the backbone ribbon drawings. The coordinates of cystatin B were extracted from the data deposited in the Protein Data Bank, with the accession code 1STF (Stubbs et al., 1994). The maximum overlay was calculated among the residues Leu^{38}−Lys^{89}, in the cystatin A sequential numbering system.

profile, as well as the chemical shift index analysis, clearly shows that there are two discrete α-helices, which are linked to each other by a type II reverse turn, comprising the residues from Lys^{24} to Leu^{27}. It has been shown that proline is found most frequently as the second residue in such a four-residue reverse turn (Chou & Fasman, 1978). Very interestingly, and somewhat intriguingly, Martin et al. (1995) concluded, in their recent structural determination of the wild-type cystatin A (stefin A) at pH 5.5, that the α-helix is in a conformation almost identical to that of the cystatin B in the papain complex. As the chemical shifts of the residues belonging to the α-helix part of the protein do not change significantly between pH 3.8 and pH 7.1, the local conformation of the helical region must be conserved within this pH range. It may be important to point out that the conformational feature found for the α-helical portion of cystatin A causes an extra hydrophobic core region to be formed among the spatially proximate hydrophobic amino acid residues, such as Leu^{27}, Leu^{38}, Ala^{59}, and Val^{87}. The newly identified hydrophobic core in cystatin A, which was not found in either cystatin B (Stubbs et al., 1990) or even in the structure of wild-type cystatin A by Martin et al. (1995), may explain the unusually high thermostability of cystatin A as compared to cystatin B (Zerovnik et al., 1992).

(B) The N-Terminal Segment. The N-terminal portion of cystatin A is also in a quite different conformation from that of cystatin B in the papain complex. This is unexpected, since the N-terminal segment of cystatin B in the papain complex is found inserted into the active site of papain (Stubbs et al., 1990). It was, however, quite surprising that the NOEs between the N- and C-termini of cystatin A, such as those between the δ-methyls and H$^{\alpha}$ of Leu^{6} and the amide protons of Gly^{97} and Phe^{98}, were unambiguously identified (Figure 11). These long-range NOEs, between these two sequentially most distant segments, fix the otherwise unrestrained N-terminal segment, comprising residues Ile^{2}−Ser^{7} (note that the Met^{1} was lost in our preparation), into a bundle of conformations within a relatively narrow range (Figure 7). Even with the current level of refinement, which only defines the N-terminus as a conformational bundle, the relative orientation of the N-terminal segment in our structure is in stark contrast with the nearly random conformation of the N-terminal segments in the solution structures of both chicken cystatin (Diekmann et al., 1993; the Ser-form, pH 5.5) and wild-type cystatin A at pH 5.5 (Martin et al., 1995). In these structures, the N-terminal peptides were in a nearly random conformation, since no NOEs between the N- and C-termini were identified under their conditions. Once again, although our NOE measurements for cystatin A were carried out at pH 3.8, there were no substantial chemical shift changes over the pH range from 3.8 to 7.1.

(C) The First Binding Loop. The solution conformation of the first binding loop, residues Gln^{46}−Gly^{50}, of cystatin A is very similar to that of cystatin B in the papain complex (Figure 12a). The conformation of the first binding loop is very important for the cystatin inhibitory active, since this loop is primarily responsible for the tight binding to proteinases (Thiele et al., 1990). The overlays of the first binding loop structures of cystatin A and B were achieved with an rms deviation of 0.78 Å for the backbone atoms, showing that the QVVAG sequence has a well-conserved conformation. The first binding loops of the wild-type cystatin A (Martin et al., 1995) and chicken cystatin (Dieckmann et al., 1993) are also quite similar to that of cystatin B. The conformation of the first binding loop of cystatin B in the papain complex should be in the ideal conformation (the *active* form) to fit comfortably into the active site cleft of papain. Therefore, the conformations of the first binding loops found for cystatin B in the papain complex (Stubbs et al., 1990), wild-type cystatin A (Martin et al., 1995), chicken cystatin (Dieckmann et al., 1993), and cystatin A$^{2-98}$ M65L are all optimized for protease binding. As pointed out by Dieckmann et al. (1993), the first binding loop of the inhibitory active Ser form of chicken cystatin *in solution* overlays better with that of cystatin B in the papain complex than with that of the crystal structure of the inactive Gly form of chicken cystatin, which has an N-segment that is eight residues shorter than the Ser form (Bode et al., 1988; Engh et al., 1993). They ascribed the conformational alteration found for the Gly and Ser forms to the crystal contact effect (Engh et al., 1993). However, the conformations of the first binding loops of the inhibitory active cystatins belong to types 1 and 2 and are essentially identical, and only the inactive Gly form of chicken cystatin has a different conformation. This fact implies that the first binding loop of the active inhibitor adopts a specific active conformation, even for different cystatins under different conditions.

(D) The Second Binding Loop. Stubbs et al. (1990) concluded that the second binding loop in cystatin B is also

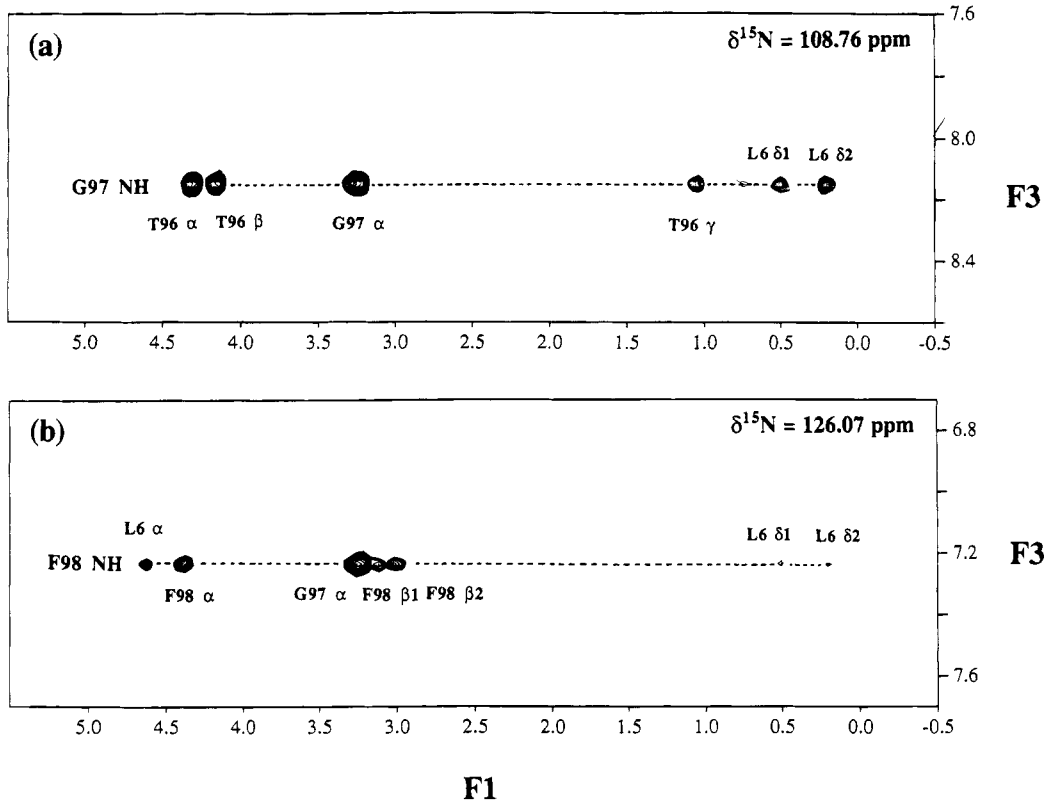

FIGURE 11: Two strips of the ^{15}N-edited NOESY-HSQC spectrum with a mixing time of 100 ms taken at the chemical shifts of residues Gly^{97} (a) and Phe^{98} (b).

involved in proteinase recognition, but to less of an extent as compared to the first binding loop. We actually collected many NOEs for this solvent-exposed loop, which allowed the second binding loop to be well defined, with residue base rms deviations of around 0.6 Å (Figure 6b). The corresponding portion of the structure of wild-type cystatin A determined at pH 5.5 was less defined (Martin et al., 1995). From the overlaid structures, shown in Figure 12b, it is clear that the local conformation of the second binding loop is significantly different from that of cystatin B; the rms deviation for the backbone atoms in the overlay of the selected portion around the second binding loop segments, Phe^{70}–Leu^{80}, was 2.2 Å. Strand E also has an apparently different conformation from the corresponding strand in cystatin B. This conformational change may be ascribed to the different orientation of the second α-helix in cystatin A from the corresponding part in cystatin B. For cystatin B in the papain complex, a 3_{10} helix exists in the second binding loop, which contacts the papain. This short helix was not found in the present solution structure of *free* cystatin A. The differential conformational rigidity found for the first and second binding loops of the cystatins in the complex with papain seems to be related to the recognition processes between the cystatins and papain. Namely, the first binding loop, with the active conformation even in the free state, should maintain its active conformation to fit properly into the active site cleft of the papain, while the second hairpin loop, which has very weak direct contacts with the papain, adapts its conformation to stabilize the direct binding interactions between the adjacent loop (the first binding loop) and the papain.

Structural and Functional Effects of the N- and C-Terminal Interactions. A significant loss of the proteinase binding activities caused by the N-terminal truncation is known for chicken cystatin, a type 2 inhibitor, but so far no such effect has been observed until very recently for the type 1 cystatins (Abe et al., 1988; Machleidt et al., 1989; Abrahamson et al., 1987; Thiele et al., 1990; Lindahl et al., 1992; Shibuya et al., 1995a). The crystal structure of cystatin B, a type 1 inhibitor, in the papain complex revealed that the N-terminal part of cystatin B inserts into the active site cleft of papain (Stubbs et al., 1990). The N-terminal peptide segment of cystatin B, residues 2–5 (cystatin A numbering), adopts a type II turn and forms a hydrophobic wedge-shaped "edge" together with the first hairpin loop on the opposite side. This hydrophobic "edge" is highly complementary to the active site cleft and seems to prevent the catalytic Cys^{25} of papain from approaching and cleaving the peptide chain (Stubbs et al., 1990). This fact, which highlights the significant role of the N-terminal segment of the cystatins in the complex formation with proteinases, may be further supported by the truncation experiments described above for chicken cystatin. The experiments to prove this hypothesis, however, have yielded rather confusing results. Truncation of up to six residues, including the highly conserved Gly^4, in the N-terminus of cystatin B has been shown to have little effect on its anti-papain activity (Thiele et al., 1990). Oryzacystatin, another type 1 inhibitor, which lacks the N-terminal 21 residues, also inhibits papain activity very efficiently (Abe et al., 1988). These results seem to indicate that the N-terminal segment is not essential for the tight binding among the type 1 inhibitors and proteinases. Recent results with cystatin A (Shibuya et al., 1995), however, which shares 54% sequence homology with cystatin B, reveal that the deletion of the first two N-terminal residues does not change the inhibitory activity, but the deletion of the residues after Pro^3 resulted in a drastic decrease in activity. Indeed, the deletion of Gly^4, the highly conserved residue among the

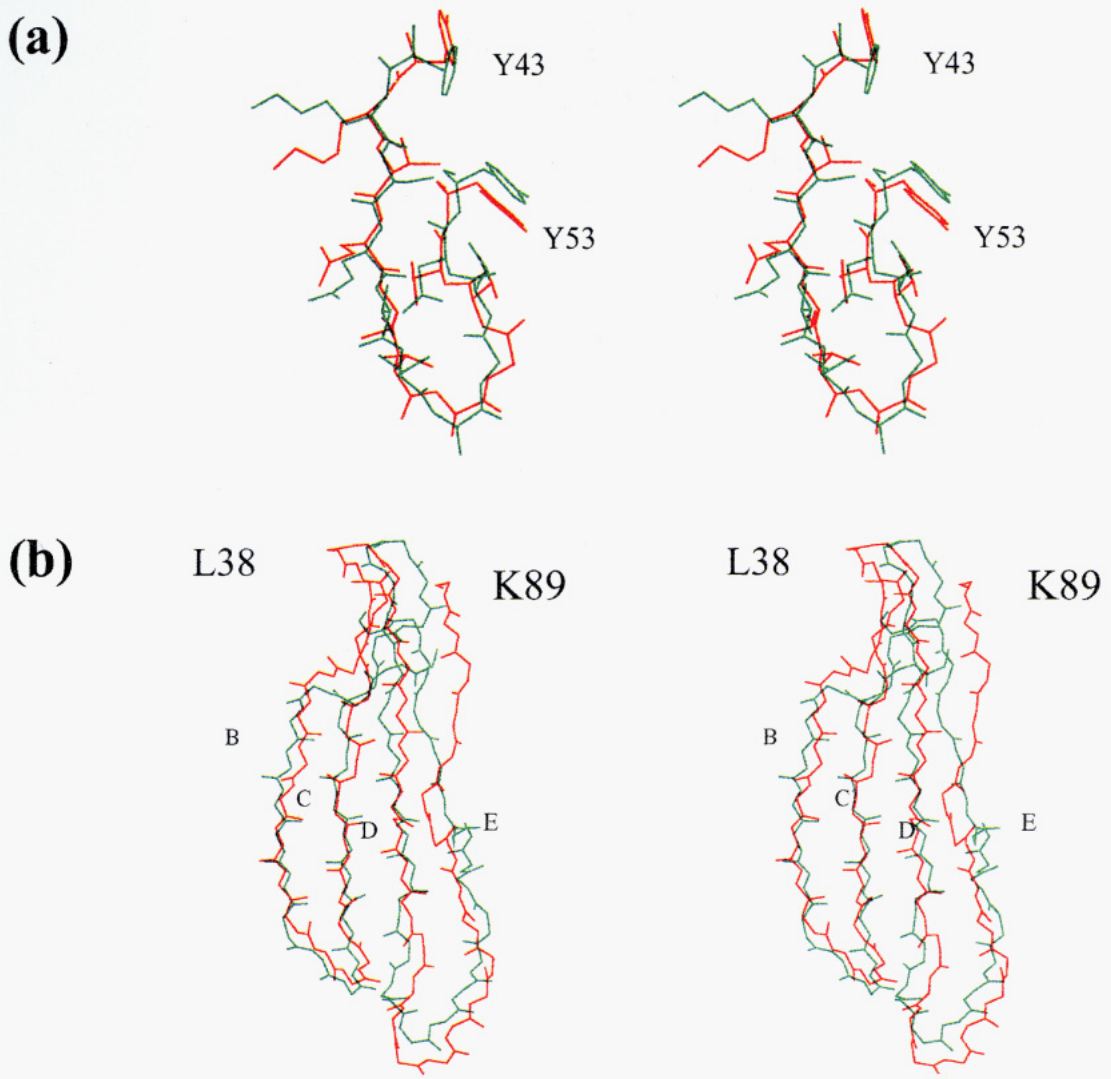

FIGURE 12: (a) Binding loop comparison. The mean coordinate of cystatin A (red) is shown superimposed with the X-ray structure of cystatin B (green). (b) Comparison of the β-sheets in the mean structure of cystatin A (red) is shown by superimposing the corresponding part of the cystatin B structure (green).

various cystatins, completely abolishes the activity of cystatin A, and no activity remains in truncations up to Glu[8] (Shibuya et al., 1995b). Even more surprisingly, a cystatin A variant with Gly[4] replaced with Val, cystatin A^{2-98} G4V M65L, shows almost no activity toward papain (Shibuya et al., 1995b). The result might be interpreted by the "N-trunk model", since the putative binding site in papain for the N-terminal segment of cystatin A may not be able to accommodate the bulky side chain of Val. This explanation is, however, not compatible with the experiments for cystatin B and oryzacystatin, which show that the N-terminal segments are not essential for inhibitory activity, as described above. In order to explain these apparently contradictory results, we have investigated the effects of N-terminal truncations on the structure of cystatin A to determine what may actually be responsible for the loss of inhibitory activity.

The $^1H-^{15}N$ HSQC spectral changes found between cystatin A (cystatin A^{2-98} M65L) and cystatin A^{5-98} provide good means of identifying the region(s) with conformational changes induced by the N-terminal truncation. The N-terminal segment of our cystatin A structure appeared as a bundle of various conformations within a relatively narrow range, which interacts with the residues at the C-terminal segment, as clearly identified by the long-range NOEs among these segments (Figure 11). As a result of these distance constraints, the N-terminal peptide chain in our structure is directed toward the C-terminus (Figure 7). In the structure reported by Martin et al. (1995), the N-terminus is not well defined and seems to be directed toward the opposite side of the C-terminus. Our observation suggests that the truncation of a few additional residues after Pro[3] from the N-terminus of cystatin A may pull the N-terminal peptide segment apart from the C-terminal region, due to the loss of such interactions that hold the otherwise distant segments together. As shown above, the $^1H-^{15}N$ HSQC spectral changes induced by the N-terminal truncation were observed not only for the residual N-terminal segment but also for the other parts, including the first binding part with the conserved QVVAG sequence and, to a smaller extent, around the C-terminus (Figure 9). The results strongly imply that the conformation of the first binding loop (the *active* conformation) in cystatin A is maintained by specific interactions between the N- and C-termini and is transformed into the *inactive* conformation by removing the N- and C-interterminal interactions. The N- and C-interterminal interactions in cystatin A can be removed also by the deletion of the C-terminus, and we actually found that cystatin A^{2-92} lost its activity, as expected (Samejima et al., unpublished results). In the cases of cystatin B (Jerela et al., 1991) and oryzacystatin (Abe et al., 1988), the C-terminal deletion has

little effect on their inhibitory activities, which shows that the N- and C-interterminal interactions are not required to maintain their active conformations.

The conformational change in the first binding loop can be induced without cleavage of either the N- or C-terminal segment. For example, a single amino acid mutant cystatin A, cystatin A^{2-98} G4V M65L (note that our cystatin A is actually cystatin A^{2-98} M65L, which is fully *active*) is inhibitory *inactive*. A large chemical shift change was observed for the $^{1}H-^{15}N$ correlation signal for Val^{47} in the $^{1}H-^{15}N$ HSQC spectrum of this mutant labeled selectively with [^{15}N]valine (Shibuya et al., 1995b), which suggests that the conformational change for the QVVAG (Val^{47} is a bold letter) sequence in the first binding loop, probably from the *active* to the *inactive* form, is triggered by this single amino acid replacement. Although one might assume that the destabilization of the N- and C-interterminal interactions may be due to the bulky Val^{4} residue in the Gly^{4} position, further NMR studies will be necessary to elucidate the molecular mechanisms of this inactivation process.

CONCLUSIONS

The role of the N-terminal segment of the cystatins in proteinase binding has been a controversial issue, even though the segment is seemingly involved in specific binding interactions with the proteinase, as shown by the X-ray analysis of the cystatin B−papain complex (Stubbs et al., 1990). The X-ray result is apparently incompatible with the results of the truncation of the N-terminal segment of cystatin B, which resulted in little loss of the inhibitory activity (Thiele et al., 1990). Although a similar binding model has been presented for the N-terminal segment of chicken cystain and papain (Turk and Bode, 1991), the activity of chicken cystatin is lost by truncating its N-terminal residues. The present studies allow us to explain the rather confusing biochemical experimental results accumulated for the cystatins over many years. It is now clear that the N-terminal segment does not necessarily play a direct role in the proteinase binding, even for the cystatins in which the N-terminal truncation leads to the loss of inhibitory activity. Taking all existing results into account, it is most reasonable to assume that the conformational alteration of the first binding loop, from the *active* to the *inactive form*, is primarily responsible for such an activity loss. Therefore, there might be perturbations other than on N-terminal truncation, which potentially diminish the inhibitory activities of the cystatins by altering the conformation of the first binding loops, such as amino acid mutation, deletion, or chemical modification.

There seems to be two groups of inhibitors belonging to the cystatin superfamily, regardless of the subfamily to which they belong. The cystatins in the first group (group I) do not require the N- and/or C-terminal segment to maintain the active conformation of the first binding loop. Cystatin B (type 1) and oryzacystatin (type 1) are in this group, for which the truncation of these two segments does not result in an activity loss, since their first binding loops adopt active conformations without these segments. The second group of cystatins (group II) includes the inhibitors that can only maintain the active conformation of the first binding loop with the assistance of the N- and/or C-terminal segments. Cystatin A (type 1) and chicken cystatin (type 2) are in this group. In cystatin A, the active conformation of the first binding loop is maintained by the interactions between its N- and C-terminal residues. Therefore, any structural modifications, such as an N- or C-terminal truncation or an amino acid replacement in these regions, which disrupt such intersegment interactions, result in the loss of inhibitory activity. There should be another molecular mechanism to maintain the active conformation of the first binding loop for chicken cystatin, although the truncation of the N-terminal segment also results in the complete loss of its inhibitory activity, since the C-terminal segment has a rigid structure with a disulfide bond, and thus direct interactions between the N- and C-temini seem to be difficult, even for the inhibitory active Ser form. It might be important to point out that, in the group II cystatins, regardless of the actual molecular mechanisms that maintain the active conformations of the first binding loops, the inhibitory activity can be abrogated by processing the N- and/or C-terminal segment. The biological implications of this newly proposed molecular switch to turn off the inhibitory activities of the group II cystatins are not yet clear. Further studies will be required to prove this hypothesis.

ACKNOWLEDGMENT

We thank Drs. Dan Garrett and Frank Delaglio at NIH for providing the PIPP/CAPP/STAPP and the nmrPipe/nmrDraw software and Drs. David S. Wishart and Brian D. Sykes (University of Alberta) for providing the CSI program used in the chemical shift index analysis. We also thank Dr. Hatanaka, at Tokyo Metropolitan Institute of Medical Science, for valuable discussions on the structure calculations with X-PLOR.

SUPPORTING INFORMATION AVAILABLE

A table listing all assigned chemical shifts and five figures showing a selected plane of the HCCH-TOCSY spectrum, two selected planes of the NOESY-CT-HSQC spectrum, all relevant chemical shift index maps, the Ramachandran plots of the 15 converged structures, and the overlay of the five ^{1}H ^{15}N HSQC spectra collected under different pH conditions (14 pages). Ordering information is given on any current masthead page.

REFERENCES

Abe, K., Emori, Y., Kondo, H., Arai, S., & Suzuki, K. (1988) *J. Biol. Chem. 263*, 7655−7659.

Abrahamson, M., Ritonja, A., Brown, M. A., Grubb, A., Machleidt, W., & Barrett, A. J. (1987) *J. Biol. Chem. 262*, 9688−9694.

Arai, S., Watanabe, H., Kondo, H., Emori, Y., & Abe, K. (1991) *J. Biochem. (Tokyo) 109*, 294−298.

Archer, S. J., Ikura, M., Torchia, D. A., & Bax, A. (1991) *J. Magn. Reson. 95*, 636−641.

Auerswald, E. A., Genenger, G., Assfalg-Machleidt, I., Machleidt, W., Engh, R. A., & Fritz, H. (1992) *Eur. J. Biochem. 209*, 837−845.

Barrett, A. J. (1987) *Trends Biochem. Sci. 12*, 193−196.

Barrett, A. J., Rawlings, N., Davies, M., Machleidt, W., Salvesen, G., & Turk, V. (1986) *Proteinase Inhibitors*, Elsevier Science Publishers BV, The Netherlands.

Bax, A., & Pochanpsky, S. S. (1992) *J. Magn. Reson. 99*, 638−643.

Bax, A., Clore, G. M., & Gronenborn, A. M. (1990a) *J. Magn. Reson. 88*, 425−431.

Bax, A., Clore, G. M., Driscoll, P. C., Gronenborn, A. M., Ikura, M., & Kay, L. E. (1990b) *J. Magn. Reson. 87*, 620−627.
Bax, A., Ikura, M., Kay, L. E., Torchia, D. A., & Tschudin, R. (1990c) *J. Magn. Reson. 86*, 304−318.
Bode, W., Engh, R., Musil, D., Thiele, U., Huber, R., Karshikov, A., Brzin, J., Kos, J., & Turk, V. (1988) *EMBO J. 7*, 2593−2599.
Brünger, A. T. (1992) *X-PLOR (Version 3.1)*, Yale University, New Haven, CT.
Brzin, J., Kopitar, M., Locnikar, P., & Turk, V. (1982) *FEBS Lett. 138*, 193−197.
Brzin, J., Kopitar, M., Turk, V., & Machleidt, W. (1983) *Hoppe-Seyler's Z. Physiol. Chem. 384*, 1475−1480.
Chou, P. Y., & Fasman, G. D. (1978) *Adv. Enzymol. 47*, 45−148.
Clore, G. M., Gronenborn, A. M., Nilges, M., & Ryan, C. (1987) *Biochemistry 26*, 8012−8023.
Dieckmann, T., Mitschang, L., Hofmann, M., Kos, J., Turk V., Auerswald, E. A., Jaenicke, R., & Oschkinat, H. (1993) *J. Mol. Biol. 234*, 1048−1059.
Driscoll, P. C., Gronenborn, A. M., Wingfield, P. T., & Clore, G. M. (1990) *Biochemistry 29*, 4668−4682.
Eggenberger, U., Schmidt, P., Sattler, M., Glaser, S. J., & Griesinger C. (1992) *J. Magn. Reson. 100*, 604−610.
Engh, R. A., Diekmann, T., Bode, W., Auerswald, E. A., Turk, V., Huber, R., & Oschkinat, H. (1993) *J. Mol. Biol. 234*, 1060−1069.
Fesik, S. W., & Zuiderweg, E. R. P. (1990) *Q. Rev. Biophys. 23*, 97−131.
Garrett, D. S., Powers, R., Gronenborn, A. M., & Clore, G. M. (1991) *J. Magn. Reson. 95*, 214−220.
Green, G. D. J., Kembhavi, A. A., Davies, M. E., & Barrett, A. J. (1984) *Biochem. J. 218*, 939−946.
Griesinger, C., & Eggenberger, U. (1992) *J. Magn. Reson. 97*, 426−434.
Grzesiek, S., & Bax, A. (1992a) *J. Am. Chem. Soc. 114*, 6291−6293.
Grzesiek, S., & Bax, A. (1992b) *J. Magn. Reson. 99*, 201−207.
Grzesiek, S., & Bax, A. (1993) *J. Am. Chem. Soc. 115*, 12593−12594.
Järvinen, M. (1978) *J. Invest. Dermatol. 71*, 114−118.
Jerala, R., Trstenjak-Prebanda, M., Kroon-Zitko, L., Lenarcic, B., & Turk, V. (1990) *Biol. Chem. Hoppe-Seyler 371* (Suppl.), 157−160.
Jerala, R., Kroon-Zitko, L., Kopitar, M., Popovic, T., & Turk, V. (1991) *Biomed. Biochim. Acta 50*, 627−629.
Kaji, H., Kumagai, I., Takeda, A., Miura, K., & Samejima, T. (1989) *J. Biochem. (Tokyo) 105*, 143−147.
Kay, L. E., Ikura, M., Tschudin, R., & Bax, A. (1990) *J. Magn. Reson. 89*, 496−514.
Kay, L. E., Keifer, P., & Saarinen, T. (1992) *J. Am. Chem. Soc. 114*, 10663−10665.
Lindahl, P., Nycander, M., Ylinenjärvi, K., Pol, E., & Björk, I. (1992) *Biochem. J. 286*, 165−171.
Machleidt, W., Borchart, U., Fritz, H., Brzin, J., Ritonja, A., & Turk, V. (1983) *Hoppe-Seyler's Z. Physiol. Chem. 364*, 1481−1486.
Machleidt, W., Thiele, U., Laber, B., Assflg-Machleidt, I., Esterl, A., Wiegand, G., Kos, J. Turk, V., & Bode, W. (1989) *FEBS Lett. 243*, 234−238.
Machleidt, W., Thiele, U., Assfalg-Machleidt, I., Förger, D., & Auerswald, E. A. (1991) *Biomed. Biochim. Acta 50*, 613−620.
Marion, D., Kay, L. E., Sparks, S. W., Torchia, P. A., & Bax, A. (1989a) *J. Am. Chem. Soc. 111*, 1515−1517.
Marion, D., Driscoll, P. C., Kay, L. E., Wingfield, P. T., Bax, A., Gronenborn, A. M., & Clore, G. M. (1989b) *Biochemistry 28*, 6150−6156.
Martin, J. R., Craven, C. J., Jerala, R., Kroon-Zitko, L., Zerovnik, E., Turk, V., & Waltho, J. P. (1995) *J. Mol. Biol. 246*, 331−343.
Muhandiram, D. R., & Kay, L. E. (1994) *J. Magn. Reson. B103*, 203−216.
Neri, D., Szyperski, T., Otting, G., Senn, H., & Wüthrich, K. (1989) *Biochemistry 28*, 7510−7516.
Nikawa, T., Towatari, T., Ike, Y., & Katunuma, N. (1989) *FEBS Lett. 255*, 309−314.
Nilges, M., Gronenborn, A. M., Brünger, A. T., & Clore, G. M. (1988) *Protein Eng. 2*, 27−38.
Nilges, M., Kuszewski, J., & Brünger, A. T. (1991) in *Computational Aspects of the Study of Biological Macromolecules by Nuclear Magnetic Resonance Spectroscopy* (Hoch, J. C., Poulsen, F. M., & Redfield, C., Eds.) pp 451−455, Plenum Press, New York.
Piatto, M., Saudek, V., & Sklenar, V. (1992) *J. Biomol. NMR 2*, 661−665.
Powers, R., Garrett, D. S., March, C. J., Frieden, E. A., Gronenborn, A. M., & Clore, G. M. (1993) *Biochemistry 32*, 6744−6762.
Shaka, S. J., Lee, C. J., & Pines, A. (1988) *J. Magn. Reson. 77*, 274−293.
Shibuya, K., Kaji, H., Itoh, T., Ohyama, Y., Tsujikami, A., Tate, S., Takeda, A., Kumagai, I., Hirao, I., Miura, K., Inagaki, F., & Samejima, T. (1995a) *Biochemistry 34*, 12185−12192.
Shibuya, K., Kaji, H., Ohyama, Y., Tate, S., Kainosho, M., Inagaki, F., & Samejima, T. (1995b) *J. Biochem. 118*, 635−642.
Stubbs, M. T., Laber, B., Bode, W., Huber, R., Jerala, R., Lenarcie, B., & Turk, V. (1990) *EMBO J. 9*, 1939−3947.
Sylvester, S. R., & Stevens, C. M. (1979) *Biochemistry 18*, 4529−4531.
Thiele, U., Assfalg-Machleidt, I., Machleidt, W., & Auerswald, E.-A. (1990) *Biol. Chem. Hoppe-Seyler 371* (Suppl.), 125−136.
Turk, V., & Bode, W. (1991) *FEBS Lett. 285*, 213−219.
Vuister, G. W., & Bax, A. (1992) *J. Magn. Reson. 98*, 428−435.
Vuister, G. W., & Bax, A. (1993) *J. Am. Chem. Soc. 115*, 7772−7777.
Wagner, G., Braun, W., Havel, T. F., Schaumann, T., Go, N., & Wüthrich, K. (1987) *J. Mol. Biol. 196*, 611−639.
Wishart, D. S., & Sykes, B. D. (1994) *J. Biomol. NMR 4*, 171−180.
Wüthrich, K. (1986) *NMR of Proteins and Nucleic Acids*, John Wiley & Sons, New York.
Wüthrich, K., Billeter, M., & Braun, W. (1983) *J. Mol. Biol. 169*, 949−961.
Zerovnik, E., Lohner, K., Jerala, R., Laggner, P., & Turk, V. (1992) *Eur. J. Biochem. 210*, 217−221.

BI951508V